Research papers

Landward shifts of the maximum accretion zone in the tidal reach of the Changjiang estuary following construction of the Three Gorges Dam

Xuefei Mei [a], Zhijun Dai [a,b,*], Stephen E. Darby [c], Min Zhang [a,d], Huayang Cai [e], Jie Wang [a], Wen Wei [a]

[a] *State Key Laboratory of Estuarine and Coastal Research, East China Normal University, Shanghai 200062, China*
[b] *Qingdao National Laboratory for Marine Science and Technology, Qingdao 266100, China*
[c] *School of Geography and Environmental Sciences, University of Southampton, Southampton SO17 1BJ, UK*
[d] *Department of Geography, Shanghai Normal University, Shanghai, China*
[e] *School of Marine Engineering and Technology, Sun Yat-sen University, Guangzhou, China*

ARTICLE INFO

ABSTRACT

Impacts from anthropogenic activities have substantially modified the geomorphology of most of the world's large rivers. While many studies have focused on the fluvially-dominated and estuarine/delta segments of these rivers, their tidal reaches that links the river to the estuarine delta is much less extensively documented. Yet, morphological variations in these key transition zones, however, directly affect the transfer of water and sediment to the sea, and have a significant influence on the delta environment. Here, we analyze the morphological variation of the Datong-Xuliujing Reach (DXR), the tidal reach of the Changjiang River, following the closure and operation of the Three Gorges Dam, using a unique dataset combining surveys in 1992, 2002, 2008 and 2013. The results demonstrate that the DXR exhibits three different morphological development phases. When sediment supply is high (at 3.18×10^8 t/y), the DXR experienced deposition (1992–2002) with the maximum accretion zone located in the middle portions of the reach. Thereafter (2002–2008) the channel underwent a major period of erosion coincident with a substantial decline of fluvial sediment supply (to 1.72×10^8 t/y). More recently (i.e., during 2008–2013), the entire reach experienced deposition, but with the maximum accretion zone shifting around 100 km landward (compared to its position in 1992–2002), while the riverine sediment supply was further reduced to 1.30×10^8 t/y. Our analytical modelling further reveals that a damped high fluvial discharge, induced by Three Gorges Dam regulation, and a relatively strong water level fluctuation induced by tidal forcing in the wet season, are responsible for the upstream shift in the maximum accretion zone. In addition, local variations caused by sand mining and dredging generate spatial nonuniformity in the observed patterns of erosion and deposition along the DXR. Such knowledge is of vital importance for the sustainable management of large alluvial rivers and their tidal reaches as they respond to natural and anthropogenic effects.

1. Introduction

The world's estuarine deltas are dynamic transition zones where rivers meet the ocean (Savenije, 2012; Nienhuis et al., 2018). Estuarine deltas are critically important environments as they provide important ecosystem services that support the lives and livelihoods of hundreds of millions of people worldwide (Ericson et al., 2006; Tessler et al., 2015; Angamuthu et al., 2018). However, as low-lying environments subject to the continually changing balance between competing fluvial and tidal processes, there is concern that they are facing a major sustainability crisis of subsidence (Syvitski et al., 2009; Lentsch et al., 2018; Dunn et al., 2019). Specifically, many of the world's estuarine deltas are sinking as a result of the extraction of water, oil and gas from the subsurface (Syvitski et al., 2009; Hoitink et al., 2017). Other human activities, such as the embankment of delta channels and the construction of dams in the river catchments that feed them (Kondolf et al., 2014; Dunn et al., 2019) are preventing the natural aggradation of delta plains, which could further exacerbate such delta lowering (Paola et al., 2011; Giosan et al., 2013, 2014). Alongside the removal of sand from channels to promote navigation and for use as building aggregate (Auerbach

---

et al., 2015; Hackney et al., 2020), these pressures are collectively changing the natural functioning of deltas. Indeed, the intensity of human interventions across the world's estuarine deltas is now so high that the morphodynamic evolution of many deltas can arguably no longer be considered natural, placing a number of deltas in greater danger of inundation due to reductions in floodplain sedimentation, accelerated subsidence and sea-level rise (Nicholls et al., 2016; Lentsch et al., 2018).

The scale of these human disturbances within, and upstream, of estuarine deltas may be expected to have significant impacts. For example, the construction of reservoirs and the subsequent operation of dams, may lead to seasonal changes in the delivery of freshwater flows that, in turn, lead to adjustments in the function of fluvial and estuarine hydrology (Poff et al., 2007; Assani et al., 2011; Mei et al., 2015). Within estuarine deltas, changes in channel (for example, due to sand mining) and delta-plain morphology (for example, due to land reclamation) are also known to have non-local impacts on changes in the tidal prism (Angamuthu et al., 2018; Bain et al., 2019), feeding back to further destabilise channel morphology. Importantly, these pressures are stressing many large rivers and their estuarine deltas, including major rivers in east and south Asia such as the Mekong River in Vietnam, the Ganges River in India, and the Pearl and Changjiang Rivers (the latter is the focus of this study) in China. Indeed, most of the world's large rivers have now been significantly dammed in their central and upper reaches, resulting in changes in hydraulics and morphological adjustments in their lower reaches (Räsänen et al., 2017; Rahman et al., 2018; Dunn et al., 2019). Moreover, these environmental stresses are expected to increase, both as a result of ongoing climate change, as well as increasing population, urbanization and socio-economic change (Darby et al., 2016; Angamuthu et al., 2018; Dunn et al., 2019). A detailed understanding of the ways in which tidal channel morphology adjusts to environmental change is, therefore, an essential pre-requisite for ensuring that the world's estuarine deltas can be managed in ways that increase their resilience.

As the longest river in Asia, the Changjiang (Yangtze) River has been subjected to extensive human interference, particularly the construction of the Three Gorges Dam (TGD) in 2003, the world's largest piece of hydraulic infrastructure (Mei et al., 2015; Dai et al., 2016). Although many previous studies have investigated the morphological response of the Changjiang since the closure of the TGD, these prior works have mainly focused on either the upstream river basin that is completely dominated by fluvial discharge (e.g. Yuan et al., 2012; Lai et al, 2017; Mei et al., 2018; Deng et al., 2019), or the estuarine delta that is directly and significantly affected by tidal asymmetry (Kuang et al., 2013; Luan et al., 2017; Zhang et al., 2018). In contrast, much less information is available on the erosion/accretion status of the tidally-influenced reach that links the river basin to the delta, much less to consider how the combined effects of dam construction and altered flow regime have affected the morphology of this critical transition zone. Located in the last 500 km of the river, the tidal reach of the Changjiang is characterized by a dynamic environment which is dominated by fluvial forcing, but affected by tidally-induced water level fluctuations. No long-term observations are available for water and sediment discharge along this tidal reach due to its complicated hydrodynamic conditions (Mei et al., 2019). The same problem exists in many other large rivers, such as the Mekong (Lauri et al., 2012) and Mississippi (Wang and Xu, 2018), which are relatively under-studied in their lowermost reaches. This situation severely hinders management of the Changjiang's estuarine delta, one of the world's economically most important, because morphological processes along the tidal reach can significantly affect the sediment budget of the entire system. This study directly fills this gap by addressing the following specific objectives: 1) To detect the morphological changes of the tidal Changjiang before and after construction of the TGD, using conventional bathymetric surveys; 2) To explore, using an analytical model, how the altered spatial–temporal hydrodynamics affect the observed morphological changes along the tidal Changjiang; 3) To identify the potential drivers of the morphological evolution in the study area. The knowledge derived from this study can be considered as an analogue for other major *meso*-tidal systems (such as the Mekong and Pearl) that have similar seasonal flow regimes and tidal ranges, and which are facing similar environmental pressures.

2. Study location

The Changjiang (Yangtze) River basin, extending 6300 km from the Tibetan Plateau to the East China Sea, covers about 20% of the total area of China (Yan et al., 2010). The specific focus of this study is the 512 km-long portion between Datong and Xuliujing (117°37′ E −121°59′ E and 30°46′ N-31°00′ N, Fig. 1A) (hereafter, DXR), the lowermost part of the Changjiang River that connects the fluvial system to the estuarine delta. Datong, as the tidal limit during the dry season, indicates the upstream most influence of tide. Downstream of Xuliujing, the Changjiang River directly branches into the estuary. Therefore, the Datong-Xuliujing reach (DXR) is distinctive from both the river and the estuary, with an obvious transition between the fluvially and tidally-dominant zones. Note that the lowermost limit of the DXR is still over 100 km away from the East China Sea, its response to the tidal forcing is mainly in terms of water level fluctuations, rather than tidal asymmetry (Mei et al., 2019).

Over the period of 1992–2013, annually there were 9×10^{11} m³ and 2.31×10^8 t of water and suspended sediment discharge, respectively, entering into the DXR through Datong (Fig. S1). Being strongly affected by the Asian monsoon climate, the river's hydrological regime is highly seasonal, with more than 70% of the flow discharge passing Datong during the wet season between May and October (Chen et al., 2016). The river planform is characterized by the interconnection of relatively straight and meandering channel patterns (Fig. 1B). The Changjiang Estuary is a *meso*-tidal system with a mean tidal range of 2.2 m at Xuliujing (Fig. S2), which is primarily the result of the semidiurnal M_2 tidal constituent, followed in importance by the S_2 and K_1 tides (Zhang et al., 2018). There is no spring/neap variation in the tidal amplitude at Xuliujing, but a slight seasonal variation is observed, with the tidal range in wet season (May to October) being on average 0.1 m higher than in the dry season (November to April) (Fig. S2). Xuliujing is dominated by the ebb tide, with average flood and ebb durations of 4.5 h and 8 h, respectively, and correspondingly, the mean flood and ebb tidal currents are 0.61 m/s and 1.02 m/s. Datong and Zhenjiang mark the approximate limits of the tidal backwater influence in the dry and flood seasons, respectively. The stations at Nanjing and Jiangyin represent the uppermost limits to which the tidal flood currents penetrate, again in the dry and flood seasons, respectively (Mei et al., 2019; the locations of these interfaces are indicated on Fig. 1B). The upper limit of the DXR is located some 1200 km downstream of the TGD (see Fig. 1A for location). The TGD project began in 2003; by 2009, when full operations began, the total water storage capacity was ~40 billion m³, equivalent to 5% of the Changjiang's mean annual discharge (Bao et al., 2015).

3. Data collection and methods

Four types of data were collected in this study: 1) topographic maps, dating from 1992, 2002, 2008 and 2013 (in each case the surveys on which the maps are based were undertaken during the wet season, i.e. between May and August), were obtained from the Changjiang Waterway Bureau and used to determine morphological changes along the DXR and to provide the geometric characteristic parameters used subsequently in the analytical model. The resolution of the bathymetric data is further introduced in Section 3.1; 2) Daily water and suspended sediment discharges at Datong were obtained from the Changjiang Water Resources Commission for the period from 1992 to 2013 (the location of Datong is indicated on Fig. 1B). Water discharge was estimated through the representative vertical line method, which divides the entire cross-section into 6 bins by 5 velocity verticals following the code for hydrologic data processing in China (The Ministry of Water
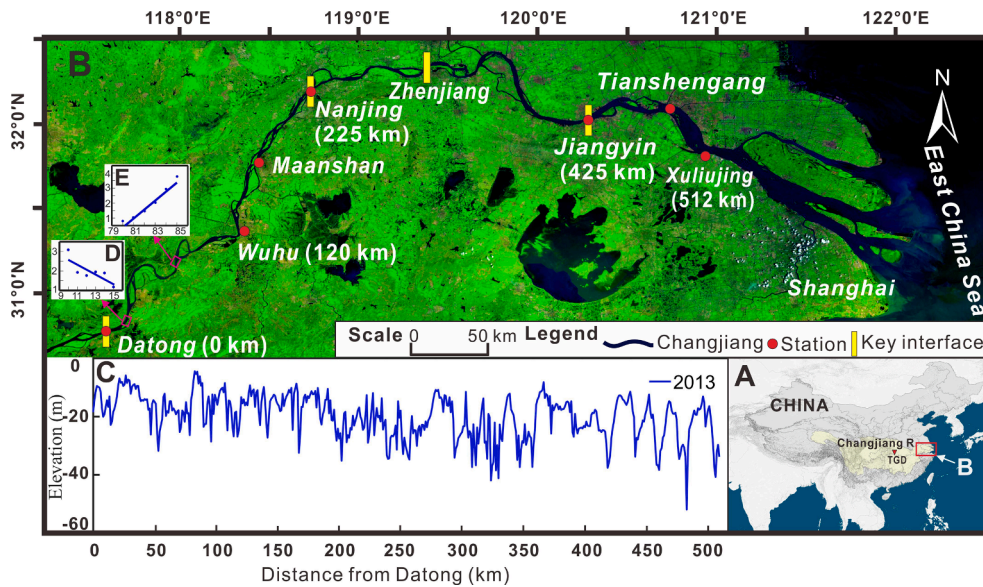
Fig. 1. Overview of the Datong-Xuliujing Reach (DXR), showing: (A) the location of the Changjiang River in China (the red box marks the location of panel B; TGD marks the location of the Three Gorges Dam); (B) the DXR showing locations of sites referred to in the text; (C) thalweg profile of the DXR as observed in 2013; (D, E) channel width variation in the selected reaches, with x-axis indicating the distance from Datong (km) and the y-axis indicating the channel width. The remote-sensing images of Fig. 1A is from USGS. The remote-sensing images of Fig. 1A is from USGS. (For interpretation of the references to colour in this figure legend, the reader is referred to the web version of this article.)

Resources of the People's Republic of China (MWRPRC), 2012). For each bin, its discharge is the product of the wetted cross-sectional area and the mean flow velocity of the corresponding representative line (Mei et al., 2019). A vertical velocity profile is measured with acoustic Doppler current profilers (ADCP). Suspended sediment discharge was obtained as the product of the discharge and suspended sediment concentration. Suspended sediment concentration in fluid is measured by filtering and drying of the samples that were obtained from horizontal suspended sediment sampler with a storage capacity of 1000 ml (The Ministry of Water Resources of the People's Republic of China (MWRPRC), 2012); 3) Hourly tidal levels, as measured at Xuliujing in 2002 and 2013, were obtained from the Changjiang Water Conservancy Committee; 4) Monthly mean tidal ranges and water levels in 2002 and 2013 at Wuhu (WH), Maanshan (MAS), Nanjing (NJ), Zhenjiang (ZJ), Jiangyin (JY), and Tianshenggang (TSG) were obtained from the Changjiang Hydrology Bureau of the People's Republic of China (the locations of these stations are indicated on Fig. 1B).

To address the issues outlined in Section 1, we firstly conducted an empirical analysis using repeat bathymetric surveys, which enabled us to quantify the evolution of the Changjiang tidal channel's morphology before and after construction of the TGD (Section 3.1). Then, we employed a well-developed analytical model (Cai et al., 2013, 2016, 2019), in a range of simulation experiments to further analyze how the changes in flow regime, channel morphology and tidal amplitude affect the spatial patterns of tide-river hydrodynamics in the wet season (Section 3.2). By combining the data obtained from both approaches we seek to link the observed changes in morphology to their causative mechanisms.

3.1. Bathymetric change analysis

To quantify the change in the morphology of the DXR before and after completion of the TGD, we employed a dataset compiled from 4 topographic maps. The maps dating from 1992 and 2002 represent the bathymetric information before the construction of TGD, while the charts from 2008 and 2013 reflect the morphological response since its subsequent closure and operation. From each map around 700–900 cross sections, spaced at a distance of around 400–600 m (this is equivalent to one cross-section for roughly every 2 to 3 channel widths based on the minimum channel width) were digitized to characterize the channel bathymetry. The cartographic data used to compile the original maps were acquired using shipborne dual-frequency echo sounders for depth measurement and GPS devices for positioning, with a vertical

error of approximately 0.2 m and a positioning error of 1 m. Such small depth and position errors highlight the high quality of the data (Dai et al., 2014). The map scales range from 1:20,000 to 1:80,000 (Table S1A–D).

The data from the maps were transferred into depth points relative to Beijing 54 coordinates and were corrected to the 'Wusong Datum' (which refers to the lowest water level) using ArcGIS. Thereafter, the vector bathymetric point data from each map were gridded using the Kriging interpolation method to generate a digital elevation model (DEM) with 50×50 m grid resolution (van der Wal et al., 2002; Blott et al., 2006). Spatial variations in deposition and erosion of the river bottom were then obtained by comparing the riverbed elevations of two adjacent (in time) surveys using:

$$\Delta h(p, t_1, t_2) = h_2(p, t_2) - h_1(p, t_1) \tag{1}$$

where $h_1(p, t_1)$ and $h_2(p, t_2)$ are, respectively, the riverbed elevations at times t_1 and t_2 at any position $p(x, y)$. In this study, the entire 512 km length of the DXR is equally divided into 20 sub-reaches, each with a downstream interval of 25.6 km. Then, the statistical characteristics of the sub-reach averaged change in bed elevation, $\Delta h(p, t_1, t_2)$, within each of these downstream intervals were analysed by fitting a Gaussian distribution, a typical pattern used in geoscience research (Montreuil et al., 2014; Dai et al., 2018), to the long-stream variations in erosion/deposition:

$$f(\Delta h) = a exp^{(-(\Delta h - b)^2 / 2c^2)} \tag{2}$$

where $f(\Delta h)$ is the probability density function of Δh, with a indicating the height of the curve's peak, b indicating the position of the center of the peak, and c indicating the standard deviation. In this way the patterns of erosion and deposition in each epoch of change were represented as statistical models (Gaussian models) with respect to distance along the reach.

3.2. Simulations of river-tide hydrodynamics

To explore how the construction and operation of the TGD may affect the spatial–temporal patterns of tide–river hydrodynamics in the DXR during the wet season, the variation of the residual (tide-averaged) water level slope in the momentum equation were calculated using the well-developed analytical model of Cai et al. (2013), Cai et al. (2016), Cai et al. (2019). Flow deceleration around the maximum residual water level slope should render a transition zone for processes of sediment

transport and deposition, with most deposition taking place around this region and thus generating a maximum sediment deposition zone (Lamb et al., 2012). This can be attributed to the sudden decrease of velocity when the water surface transitions from a steep to more gentle gradient. The performance of this analytical model in the Changjiang Estuary has been compared with the numerical TELEMAC model that considers both the real bathymetrical condition and time varying inputs. The results of this comparison exercise showed that the two models are consistent in reproducing the seasonal behavior of tide–river dynamics and estimating the residual water level profile for a wide range of tide and river discharge scenarios (Zhang et al., 2016), demonstrating that the simpler analytical model can be used with confidence in this study.

3.2.1. Basic equations for reproducing the residual water level profile

In tidal rivers, the cross-sectional averaged residual water level can be obtained from the one-dimensional momentum equation (Savenije, 2012; Cai et al., 2016):

$$\frac{\partial U}{\partial t} + U\frac{\partial U}{\partial x} + g\frac{\partial Z}{\partial x} + \frac{gh}{2\rho}\frac{\partial \rho}{\partial x} + g\frac{U|U|}{K^2 h^{4/3}} = 0 \tag{3}$$

where U is the cross-sectional averaged velocity, Z is the free surface elevation, h is the water depth, g is the acceleration of gravity, t is time, ρ is the water density, x is the distance along the channel (starting from the estuary), and K is the Manning-Strickler friction coefficient. Assuming a periodic variation of flow velocity, the residual water level slope can be calculated as (Cai et al., 2019):

$$\overline{\frac{\partial Z}{\partial x}} = -\frac{1}{K^2}\overline{\left(\frac{U|U|}{h^{4/3}}\right)} - \frac{1}{2g}\frac{\partial \overline{U^2}}{\partial x} - \frac{1}{2\rho_0}\overline{h\frac{\partial \rho}{\partial x}} \tag{4}$$

where the over bars and the subscript zero, respectively, indicate the tidal average and the value at the seaward boundary. As Eq. (4) indicates, the residual water level slope is governed by the residual friction, the advective acceleration, and density effects. Compared to the frictional dissipation, the contribution of advective acceleration and density effects have been shown to be rather small in the Changjiang Estuary (Savenije, 2012; Cai et al., 2019), Eq. (4) can, therefore, justifiably be further integrated to:

$$\overline{Z}(x) = -\int_0^x \overline{\frac{\partial Z}{\partial x}}dx = -\int_0^x \overline{\frac{U|U|}{K^2 h^{4/3}}}dx \tag{5}$$

Here we set the residual water level at the estuary mouth ($x = 0$) as 0.

3.2.2. Analytical solution for tide-river dynamics

To derive the residual water level profiles in the estuary, the longitudinal variation of cross-sectional area and width are both assumed follow an exponential function (see Toffolon et al., 2006; Cai et al., 2016 for justification):

$$\overline{A} = \overline{A_r} + (\overline{A_0} - \overline{A_r})\exp(-\frac{x}{a}) \tag{6}$$

$$\overline{B} = \overline{B_r} + (\overline{B_0} - \overline{B_r})\exp(-\frac{x}{b}) \tag{7}$$

where $\overline{A_0}$ and $\overline{B_0}$ are the tidally averaged cross-sectional area and width at the estuary mouth; $\overline{A_r}$ and $\overline{B_r}$ are the asymptotic riverine cross-sectional area and width; and the parameters a and b represent the convergence lengths of the cross-sectional area and width. Here, by assuming that the cross-section approximates a rectangular shape, the tidally-averaged depth can then be calculated directly using $\overline{h} = \frac{\overline{A}}{\overline{B}}$.

For a predominantly tidal constituent with frequency ω, the tide-river hydrodynamics is mainly determined by four dimensionless parameters: the dimensionless tidal amplitude ξ (representing the boundary condition at the seaward side), the estuary shape number γ (representing the cross-sectional area convergence), the friction number

χ (representing the frictional dissipation) and the dimensionless river discharge φ (representing the influence of freshwater discharge imposed at the upstream boundary). Detailed definitions of these four parameters are shown in Table S2.

The analytical solution for the main tide-river dynamics is obtained by solving a set of four dimensionless equations (Cai et al., 2019):

1) The damping/amplification equation,

$$\delta = \mu^2(\gamma\theta - \chi\mu\lambda\Gamma)/(1 + \mu^2\beta) \tag{8}$$

where θ, β and Γ account for the effect of river discharge and are given by:

$$\theta = 1 - (\sqrt{1+\zeta} - 1)\varphi/(\mu\lambda) \tag{9}$$

$$\beta = \theta - r_S\zeta\varphi/(\mu\lambda) \tag{10}$$

$$\Gamma = \frac{1}{\pi}[p_1 - 2p_2\varphi + p_3\varphi^2(3 + \mu^2\lambda^2/\varphi^2)] \tag{11}$$

Note that Γ is a friction factor obtained by using the Chebyshev polynomial approach (Dronkers, 1964), where the Chebyschev coefficients p_i ($i = 0, 1, 2, 3$) are functions of the dimensionless river discharge φ through $\alpha = \arccos(-\varphi)$:

$$p_0 = -\frac{7}{120}\sin(2\alpha) + \frac{1}{24}\sin(6\alpha) - \frac{1}{60}\sin(8\alpha) \tag{12}$$

$$p_1 = \frac{7}{6}\sin(\alpha) - \frac{7}{30}\sin(3\alpha) - \frac{7}{30}\sin(5\alpha) + \frac{1}{10}\sin(7\alpha) \tag{13}$$

$$p_2 = \pi - 2\alpha + \frac{1}{3}\sin(2\alpha) + \frac{19}{30}\sin(4\alpha) - \frac{1}{5}\sin(6\alpha) \tag{14}$$

$$p_3 = \frac{4}{3}\sin(\alpha) - \frac{2}{3}\sin(3\alpha) + \frac{2}{15}\sin(5\alpha) \tag{15}$$

2) The phase lag equation

$$\tan(\varepsilon) = \lambda/(\gamma - \delta) \tag{16}$$

3) The scaling equation

$$\mu = \frac{\sin(\varepsilon)}{\lambda} = \frac{\cos(\varepsilon)}{\gamma - \delta} \tag{17}$$

4) The wave celerity equation

$$\lambda^2 = 1 - \delta(\gamma - \delta) \tag{18}$$

The main dependent parameters are also described in Table S2, including the amplification/damping number δ, which indicates the rate of increase ($\delta > 0$) or decrease ($\delta < 0$) of the along-channel tidal wave amplitude; the velocity number μ, which indicates the ratio of the actual velocity amplitude to the reference value in a frictionless prismatic channel; the celerity number λ, which indicates the ratio of the classical wave celerity (c_0) to the actual wave celerity (c); and ε, which indicates the phase lag between high water and high water slack or between low water and low water slack.

To reproduce the tide-river dynamics for the entire channel correctly, the reach was sub-divided into multiple segments to account for the longitudinal variations of the cross-sections. Thus, the tidal amplitude at any distance Δx upstream of the seaward boundary was obtained by simple explicit integration for a given tidal amplification/damping number δ and tidal amplitude η_0 at the seaward boundary:

$$\eta_1 = \eta_0 + \frac{d\eta}{dx}\Delta x = \eta_0 + \frac{\eta_0\omega\delta}{c_0}\Delta x \tag{19}$$

Based on the computed tidal amplitude and the geometric features of the next reach, the main tidal dynamics, including the amplification/ damping number, velocity number, celerity number and phase lag, were obtained by solving the set of Eqs. (8), (16)–(18).

3.2.3. Model set-up

The analytical model for the Datong-Xuliujing Reach (DXR) was set-up using three groups of data as follows: (1) geometric characteristics of the channel, including the cross-sectional area and channel depth, were used to obtain the representative exponential functions (Eqs. (6) and (7)); (2) model boundary conditions, including the seaward tidal amplitude at Xuliujing and landward fluvial discharge at Datong, were used to drive the model, and; (3) observed tidal amplitude and residual water levels for the main stations along the DXR were employed for model calibration and verification.

3.2.4. Calibration and verification of the analytical model in the Datong-Xuliujing reach

The analytical model for the DXR extends over a length of 512 km. The geometric characteristics along the DXR for the pre- and post-TGD periods, respectively, were extracted from the DEM in 2002 and 2013, at intervals of 5 km. It is evident that both the cross-sectional area and stream width are well represented by Eqs. (6) and (7), which converge exponentially toward a constant cross-section landward in the river part with a statistically significant correlation ($p < 0.05$; Fig. S3 and Table S3).

The analytical model was calibrated and verified against the observed tidal amplitude and residual water level along the DXR on the basis of the monthly mean hydrological data (including tidal ranges and water levels) in 2002 and 2013. The seaward tidal amplitude at Xuliujing, and the landward fluvial discharge at Datong for these two time periods are displayed in the Supplementary Information (Fig. S2 and S4). As the Changjiang estuary is characterized by a semi-diurnal tide, the predominant M_2 tidal period (12.42 h) was used in the analytical model. The storage width ratio r_S was set to a value of 1 for simplification, indicating negligible influence of storage area on tidal dynamics (Cai et al., 2013, 2019). Thus, the only calibration parameter is the Manning-Strickler friction coefficient, K. In 2002, the calibrated value of K was 85 $m^{1/3}s^{-1}$ in the seaward region ($x = 0$–70 km), decreasing to 50–85 $m^{1/3}s^{-1}$ over the transitional reach ($x = 70$–90 km), and then a further reduction to 50 $m^{1/3}s^{-1}$ in the landward region ($x = 90$–512 km). In 2013, the calibrated value of K was 75 $m^{1/3}s^{-1}$ in the seaward region ($x = 0$–70 km), decreasing to 43–75 $m^{1/3}s^{-1}$ over the transitional reach ($x = 70$–90 km), and finally to 43 $m^{1/3}s^{-1}$ in the landward region ($x = 90$–512 km). Although the parameter K here is in

effect a 'catch-all' calibration parameter (reflecting not only the river bed friction, but also wind forcing, the sinuosity of the channel, and so on; Cai et al., 2020), it is nevertheless noteworthy that value of K decreases in the landward direction, which is consistent with observed spatial variations in the bottom sediment grain size (the bed-material grain size being finer in the seaward areas). Note also that the calibrated value of K decreases during the period 2002–2013, which is consistent with the bed coarsening along the tidal reach.

The modeled tidal amplitude and residual water level were compared against observations at Wuhu (WH), Maanshan (MAS), Nanjing (NJ), Zhenjiang (ZJ), Jiangyin (JY), and Tianshenggang (TSG) through analysis of the Pearson product-moment correlation coefficient (Fig. 2). It can be seen that for both the tidal amplitude and residual water level, all the correlation coefficients exceeded 0.99, suggesting that the analytical model accurately reproduces the tide-river dynamics along the DXR.

4. Scenario settings

The calibrated analytical models before and after the operation of the TGD are used to run for a range of simulation experiments, in which the boundary parameters driving the river-tide hydrodynamics were varied and were calculated based on the observations during 1992–2013. Details of the methods used to compute these key parameter values for the pre- and post-TGD periods of interest are provided as follow:

4.1. Upstream boundary at Datong

To simulate the river-tide hydrodynamics, the analytical model requires a time-invariant reference discharge (specified here for the upstream limit of the DXR, at Datong). In this study we conducted simulations using three different reference discharges, based on: (i) the effective discharge; (ii) the 50th percentile (Q50) and; (iii) the 75th percentile (Q75) thresholds of the daily discharge series. In all three cases these flow discharges werecalculated based on the daily water and sediment discharge time-series at Datong over the periods 1998–2002 and 2009–2013, to represent the pre- and post-TGD evolutionary stages, respectively.

Note that the effective discharge is defined as the stream flow that transports the largest amount of sediment over geomorphic timescales (Wolman and Miller, 1960). The long-term geomorphic effectiveness of a given discharge is, therefore, the product of the flow frequency ($f(Q)$) and the suspended sediment transport rate ($S(Q)$) assigned to that flow (Q) (Doyle et al., 2005; Bunte et al., 2014). The discharge that corresponds to the peak of the product function $E(Q) = f(Q) \times S(Q)$, is thus
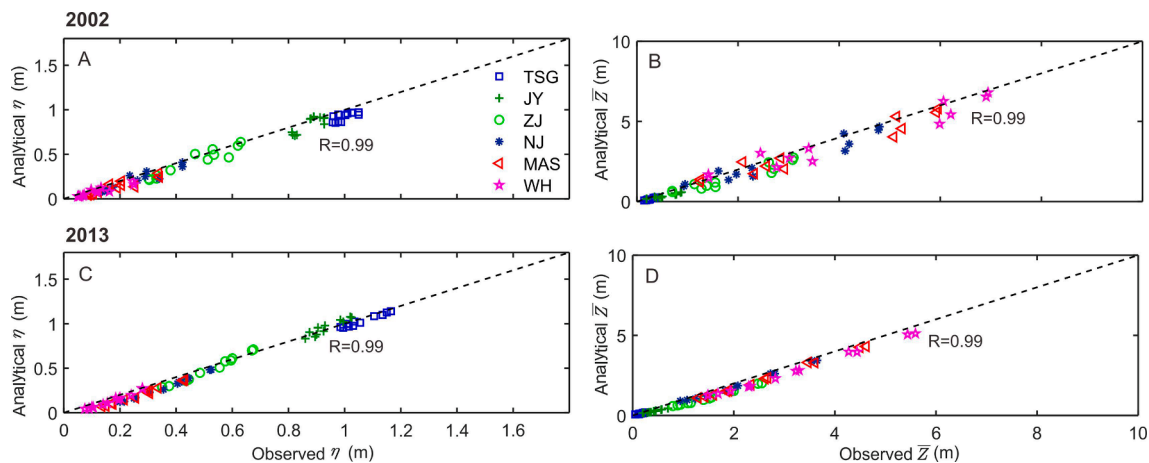
Fig. 2. Model calibration and verification through comparisons between modeled results and observations for the periods before and after the operation of the Three Gorges Dam. Comparison of (A) tidal amplitude and (B) residual water level against observations along the DXR in 2002; comparison of (C) tidal amplitude and (D) residual water level against observations along the DXR in 2013. The values of R indicate the correlation coefficient scores for the modelled versus observed data.

defined as the effective discharge. The frequency ($f(Q)$) and the suspended sediment function ($S(Q)$) that correspond to various discharge magnitudes were calculated using power functions as illustrated in (Fig. 3A-B, D-E). In this way, the effective discharges were estimated to be 47100 m³/s and 40100 m³/s, respectively, for the pre- and post-TGD periods (Fig. 3C, F; Table 1). In addition, the Q50 and Q75 during the pre- and post-TGD stages were computed to have values of 28000 m³/s and 41200 m³/s for the pre-TGD scenario; versus 23300 m³/s and 37800 m³/s for the post-TGD scenario (Table 1).

4.2. Downstream boundary at Xuliujing

The tidal amplitude at the downstream limit of the DXR was obtained using the hourly tide level at Xuliujing station. Specifically, observations in 2002 and 2013 were selected to represent the pre- and post-TGD scenario, respectively, because the tides in the Changjiang estuary are approximately the same over each spring-neap tidal cycle (Zhang et al., 2016). During the simulation experiments using the different flow discharge inputs (see 4.1) to represent the pre- and post-TGD scenarios, the downstream boundary at Xuliujing was set as the synchronous monthly mean tidal amplitude over the wet season. We focus on the tide-river hydrodynamics during the wet season as it is assumed that the channel dynamics are shaped during higher flows, and because the channel bathymetric data used to represent the channel morphology was collected at this time of year. The specified tidal amplitudes were estimated as 1.04 m and 1.12 m for the pre- and post-TGD scenarios, respectively. An overview of all the simulation experiments that were performed using the the analytical model are shown in Table 1.

Table 1
Overview of the simulation experiments in the analytical model.

Scenario	Channel morphology	Upstream boundary (m³/s)	Downstream boundary (m)
Pre-TGD	2002	Effective discharge: 47,100 Q50: 28,000 Q75: 41,200	1.04
Post-TGD	2013	Effective discharge: 40,100 Q50: 23,300 Q75: 37,800	1.12

5. Results

5.1. Erosion and accretion in the Datong-Xuliujing reach during 1992–2002

According to measurements made at Datong station, the Changjiang River annually transported 3.18×10^8 t of suspended sediment to the DXR during the period 1992–2002 (Fig. S1). Meanwhile, during this same period, our bathymetric change analysis reveals that the DXR showed clear evidence of accretion (Fig. 4), at a mean rate of 0.04 m/y (Fig. 5A). In total, the reach experienced net deposition of 0.75×10^8 t/ y, which is the equivalent of 23.6% of the annual load passing through Datong. The deposition in this period resulted in a rising of the thalweg (Fig. S5) as well as a reduction in the cross-section area of the channel (Fig. S6). Especially in the vicinity of Wuhu and Nanjing, the mean elevation aggraded by 4.42 m and 5.73 m during 1992–2002,
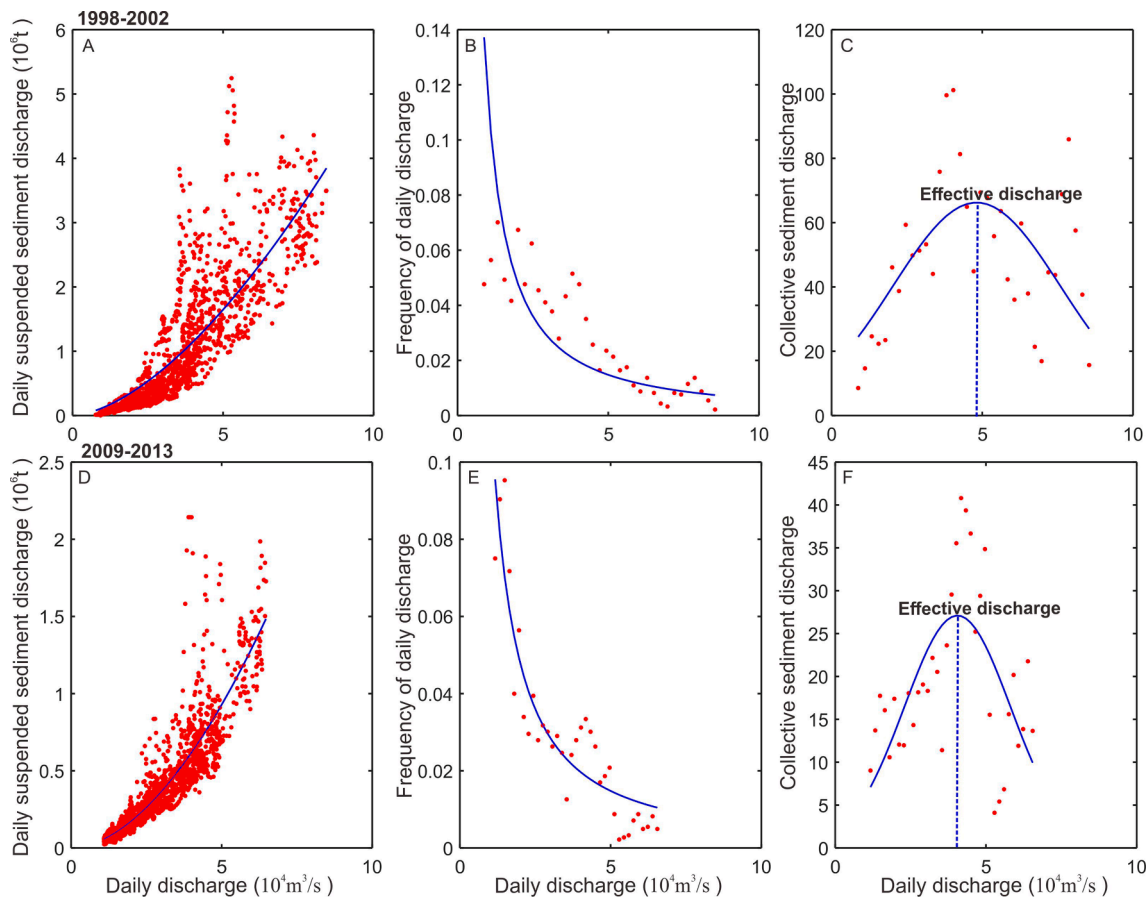
Fig. 3. Derivation of effective discharge histogram (C, F) from sediment load rating curves (A, D) and flow frequency (B, E) for the scenarios before and after the operation of the Three Gorges Dam.
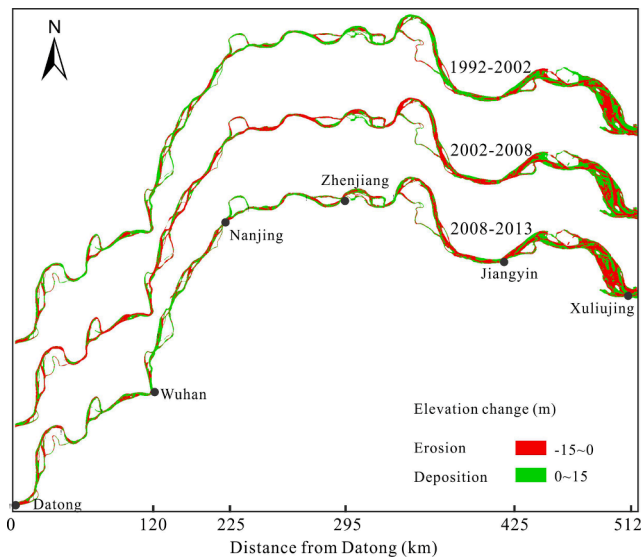
Fig. 4. Bathymetric change maps indicating patterns of erosion and deposition along the DXR for three epochs between 1992 and 2013.

respectively (Fig. S6A-B). Regarding the spatial pattern of bed accretion, there is a notable peak at the upstream limit of the reach, some 50–80 km downstream from Datong. However, when this outlier is excluded, the pattern of deposition with distance along the DXR conforms to a statistically significant (p < 0.05) Gaussian distribution with distance along the channel, with the time-averaged rate of riverbed deposition a maximum (~0.13 m/y) in the vicinity of Nanjing, which is some 230–280 km downstream from Datong (Fig. 5A). The computed Gaussian fit has a standard deviation of 2.35 sub-reaches, revealing that 68% of this zone of maximum deposition is located within a band between 200 and 320 km downstream of Datong.

5.2. Erosion and accretion in the Datong-Xuliujing reach after 2003

Following closure of the TGD in 2003, the suspended sediment load at Datong abruptly decreased from 2.06×10^8 t in 2003 to 1.32×10^8 t in 2008, stabilizing at a value of around 1.30×10^8 t thereafter (Fig. S1B). At the same time the channel also experienced riverbed scour throughout its length (Fig. 4), at an overall (along the full DXR) time-averaged erosion rate of 0.03 m/y during 2002–2008 (Fig. 5B), but with the mean bed elevation at Wuhu and Nanjing down-cutting by 5.24 m and 6.48 m, respectively (Fig. S6A-B). Furthermore, during this erosional phase there is (unlike for the pre-TGD period) there is no systematic spatial structure evident in the spatial pattern of morphological change along the reach.

In the subsequent 5 years from 2008 to 2013, almost the entire DXR again experienced channel aggradation, except in the reach downstream of Jiangyin, which underwent down-cutting (Fig. 4). The average deposition rate of the DXR during this period was 0.07 m/y (Fig. 5C), when the river bed elevations at Wuhu and Nanjing, respectively, increased by 5.81 m and 1.07 m (Fig. S6A-B). Similar to the pre-TGD period (1992–2002), and neglecting the extremely low deposition zone, located some 180–230 km downstream from Datong, as well as the zone of erosion in the distal part of the reach, the spatial pattern of riverbed deposition during 2008–2013 again is seen to conform well to a Gaussian distribution, but with the zone of maximum accretion now located close to Wuhu, some 130–180 km downstream of Datong, indicating a landward shift of ~100 km compared with the pre-TGD period (Fig. 5C). In this most recent time interval, the standard deviation around the Gaussian distribution increases slightly to 2.42 sub-reaches, indicating that 68% of this zone of observable deposition is located within a band between 120 and 250 km downstream of Datong.

5.3. River-tide dynamics along the Datong-Xuliujing reach

The interactions between tide and river flow along the DXR were simulated using the analytical model in terms of the residual (tide-averaged) water-level slope. The model results, corresponding to an effective discharge of 47000 m³/s (pre-TGD) and 40000 m³/s (post-TGD) under wet season tidal amplitudes of 1.04 m (pre-TGD) and 1.12 m (post-TGD) are illustrated in Fig. 6. It is shown that the river-induced residual water level gradient in the pre-TGD period is considerably larger than in the post-TGD phase, in part due to the larger fluvial discharge input in the pre-TGD period, and in part to the increase in the tidal amplitude (Fig. S2, S4). The river-tide interaction induced residual water level gradient is only evident in the lower reach, around 450–512 km from the Datong (Fig. 6). As the tide propagates upstream, the tidal amplitudes attenuate, becoming very small at a location approximately 300 km from Datong (Fig. 6). River forcing therefore dominates the dynamic process of much of the tidally-influenced DXR in both scenarios.

The model results also show that there is a critical location along the DXR, at which the residual water level slope is maximized. Specifically, in the pre-TGD stage, the longitudinal water level gradient profile reaches its highest value of 2.21×10^{-5} at a location some 246 km downstream of Datong (Fig. 6A). In post-TGD period, however, the location of the maximum residual water level slope (at a much smaller value of 0.93×10^{-5}) occurs much further upstream, at a location 143 km downstream of Datong (Fig. 6B). It is apparent that the locations of the model-simulated maximum residual water level slopes coincide closely with the locations of the high deposition zones observed during both the pre- and post-TGD periods (Fig. 6B, D).

Similar to the calculation of sub-reach averaged riverbed elevation change, the mean residual water level slopes for the 20 sub-reaches are obtained for the depositional phases in Fig. 7A and 7C. It is found that the longitudinal distribution of the residual water level slopes is statistical significantly (p < 0.05) correlated with the morphological changes for the river dominated reach, namely, the first 17 sub-reaches extending to around 435 km downstream of Datong (Fig. 7B, 7D), when the abnormal morphological changes are excluded according with the former parts (see 5.1 and 5.2). This phenomenon suggests the dominance of dynamics to the channel morphology. Besides, the total level of residual water level slope for the post-TGD period is substantially below pre-TGD period due to a damped high fluvial discharge and a relatively strong water level fluctuation, which in favor of sediment settlement and thus contributes to the significant accretion during 2008–2013.

6. Discussion

6.1. The effect of river morphology

The geometric characteristics of a tidal reach to a large extent determine the propagation of the tidal wave and hence the sediment transport dynamics (Zhou et al., 2018; Zhang et al., 2019). Before the construction of TGD, there was a sufficient suspended sediment supply of 3.18×10^8 t/y from the river (Fig. S1B), which generated overall deposition along the DXR, albeit with some localized areas of erosion. Specifically, erosion was evident in the reach ~ 20–30 km downstream of Datong, where the channel width decreases by over 35% from 3.07 km to 1.98 km (Fig. 1D). The sudden shrinkage of the channel likely generates a different velocity distribution and as a result, riverbed erosion (Rouse, 1961). On the contrary, there was a significant deposition around 60–80 km downstream of Datong, where the channel makes a dramatic U-turn, coupled with a sudden channel widening from 1.34 km to 4.27 km, making the reach a naturally depositional environment (Fig. 1E). The channel downstream of this high deposition zone shows a typical Gaussian profile in terms of the pattern of morphological variation with respect to distance along the channel, due to the river-tide interaction, which is further explained in Section 6.2.
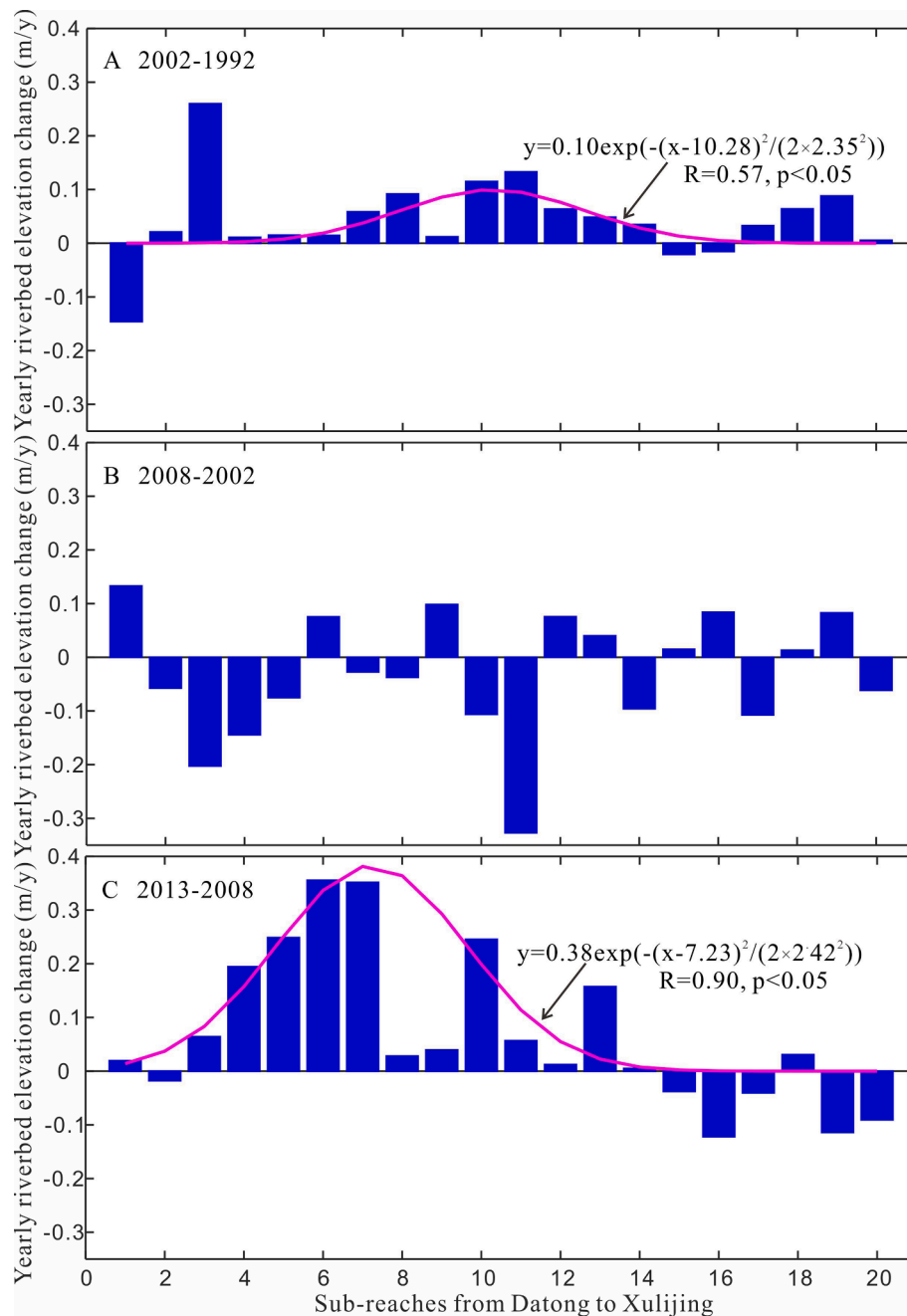
Fig. 5. Bathymetric changes observed along the Datong-Xuliujing Reach (DXR) during the period 1992–2013. For ease of description, the entire DXR is equally divided into 20 sub-reaches between Datong and Xuliujing at intervals of 25.6 km: (A) annual rate of river bed elevation change during the period 1992–2002; (B) annual rate of river bed elevation change during 2002–2008; and (C) annual rate of river bed elevation change during 2008–2013.

Following the construction of the TGD, fluvial sediment supply decreased by 45.9% to 1.72 t/y during 2003–2008, whereas the water discharge only decreased by around 10% (Fig. S1). However, siltation still can be detected, particularly around the area where the channel width suddenly increases, indicating the effects of sediment decline can be modulated by local channel planform variations. However, the entire DXR shifted to a depositional state again during 2008–2013, when the suspended sediment input to the DXR was stable at a value of around 1.30 t/y. Owning to channel resistance (Calle et al., 2017), a stable armor layer can be formed in the surface of the river bed (Lai et al., 2017), which prevents further channel degradation and contributes to morphological recovery. Consequently, the morphological evolution again follows the Gaussian pattern with respect to distance along the channel.

6.2. Interaction between runoff and tidal impacts

As a tide propagates into the tidal reach, river discharge attenuates the effects of the tidally-induced water level oscillation, but in a way that is strongly related to the pattern of morphological evolution along the estuary (Lamb et al., 2012; Leonardi et al., 2015). In this study, the relative contributions of the tide-induced water level oscillation and river discharge along the DXR are further discussed by considering various scenarios in the analytical model (Table 1). We focus on the mean-high discharge inputs, as they are the main contributors for sediment transport in the Changjiang River (Dai et al., 2016).

Two scenarios, corresponding to the normal (Q_{50}) and flood (Q_{75}) discharge conditions, respectively, are examined for both the pre- and post-TGD stages (Fig. 8). As Fig. 8A indicates, during the pre-TGD stage,
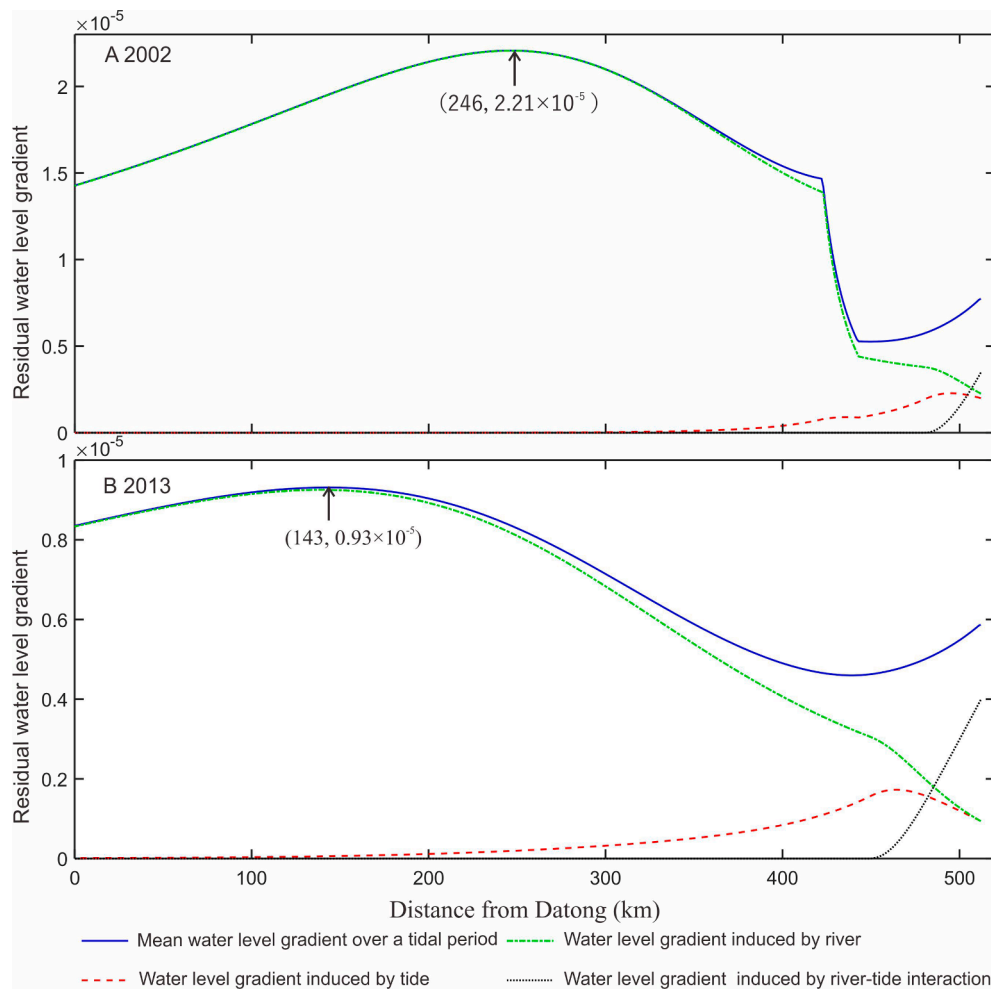
Fig. 6. Longitudinal variation of the residual water level slope, and the contributions of tidal and riverine forcing to the residual water level slope along the Datong-Xuliujing Reach for scenarios representing: (A) the period prior to operation of the Three Gorges Dam and (B) the period after the operation of the Three Gorges Dam. Thehe vertical solid lines show the location of the maximum residual water level gradient in each scenario.

the residual water level slope increased to a maximum value of 1.36×10^{-5} at a location 180 km downstream of Datong, reducing thereafter in the normal flood condition (28000 m³/s) following the deceleration of the river flow and the growing dominance of the water level fluctuation induced by the tidal wave. The slope profile under flood conditions (41200 m³/s) reaches a maximum gradient at a location 230 km downstream of Datong, indicating some 50 km of seaward shifting and an increase in magnitude of the slope of 0.6×10^{-5} (Fig. 8B). The residual water level slope behaves in a similar way in the post-TGD phase. When the river discharge input at Datong increases by 38.4% between the flood (23300 m³/s) and high flood (37800 m³/s) scenarios, the occurrence of the maximum residual water level slope migrates 47 km downstream, with the magnitude increasing by 0.4×10^{-5} (Fig. 8C-D), indicating that the relative intensity of the river and tidal forcing has the potential also to affect the location of the high deposition zone (because the convergence of the slope to its maximum value would favor sediment deposition in that location). In the high flow scenario, the effect of the tide is relatively weak, thus facilitating sediment deposition further downstream, as well as in the high deposition zone. On the contrary, the tidal influence is relatively strong in the low flow case, so that the location of the flow spreading and high deposition zone exhibits a landward migration as the tide propagates further upstream (Sassi and Hoitink, 2013).

6.3. Local mining and dredging

The evolution of the DXR is also affected directly by human activities, notably, local mining and dredging that directly force changes in the channel morphology (Zheng et al., 2018). The riverbed of the DXR comprises mainly medium-fine sand (Fig. 9), a material which has beneficial characteristics to many industries, but particularly as a construction material. Sand extraction was widespread in the middle and lower Changjiang River in the 1990s, when the channel lost as much as 80 Mt of sediment annually (Du et al., 2016). Commercial sand mining along the lower and middle Changjiang River has declined since 2003 due to stronger regulation, with the total amount of sand extraction since then being restricted to 14 Mt/yr (Chen et al., 2006). However, the actual quantity of sand mining has very likely been considerably larger than the allowed amount due to illegal extraction. For instance, in a small area 30 km upstream of Xuliujing, a total amount of 9.75 Mt of sand disappeared in half a year from November 2011 to July 2012 (Liu et al., 2014), inducing severe erosion of the riverbed and increased the channel capacity, destroying the Gaussian pattern of morphological variation noted along the reach (Fig. 5C).

Moreover, intensive dredging operations are carried out along DXR for the purpose of improving and maintaining the navigation channels, which is another human interference that further accelerates channel down-cutting (Best, 2018). According to the plan of the 12.5 m Deep-Water Channel Project, the reach downstream of Nanjing should be deepened to 12.5 m to improve navigable capacity (Fig. 1B). The
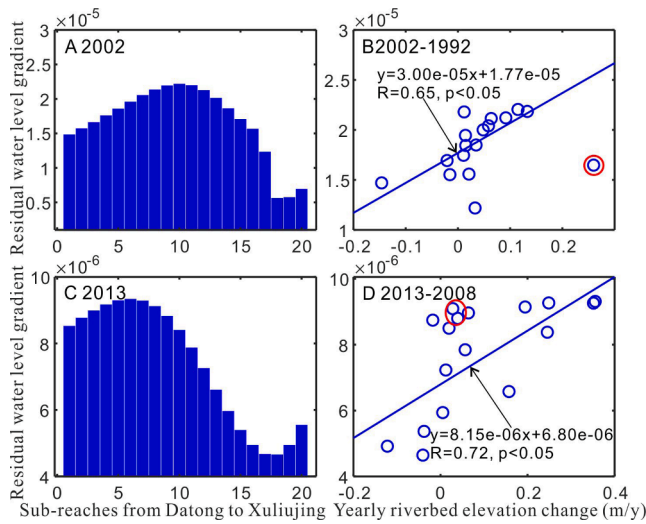
Fig. 7. Residual water level gradient simulated along the Datong-Xuliujing Reach (DXR): (A) for 2002; (C) for 2013; and relationship between simulated residual water level gradient and the observed yearly riverbed elevation change along the fluvial dominated reach during (B) 2002–1992 and (D) 2013–2008 (the blue line denotes the best fitting line). Red cycle indicates morphological change outliers that are not considered in the correlation analysis. (For interpretation of the references to colour in this figure legend, the reader is referred to the web version of this article.)

implementation of this project caused an annual loss of 11.75×10^6 m^3 of sediment from downstream of Nanjing during the period 2012–2016 (Fig. S7). In comparison to 2003, before the impoundment of the TGD, the averaged waterway depth and width of the DXR has respectively increased by 1.48 m and 200 m by 2015 (Yang et al., 2019), resulting in severe riverbed erosion and a landward moving of the deposition peak.
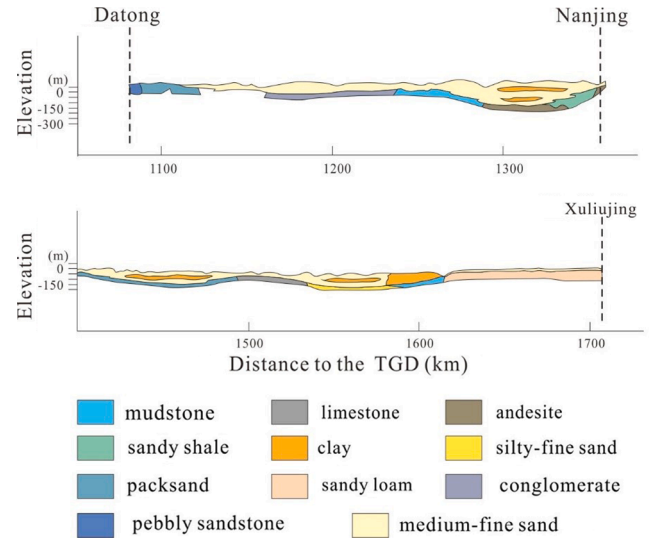
Fig. 9. Riverbed profile along the Datong-Xuliujing Reach.
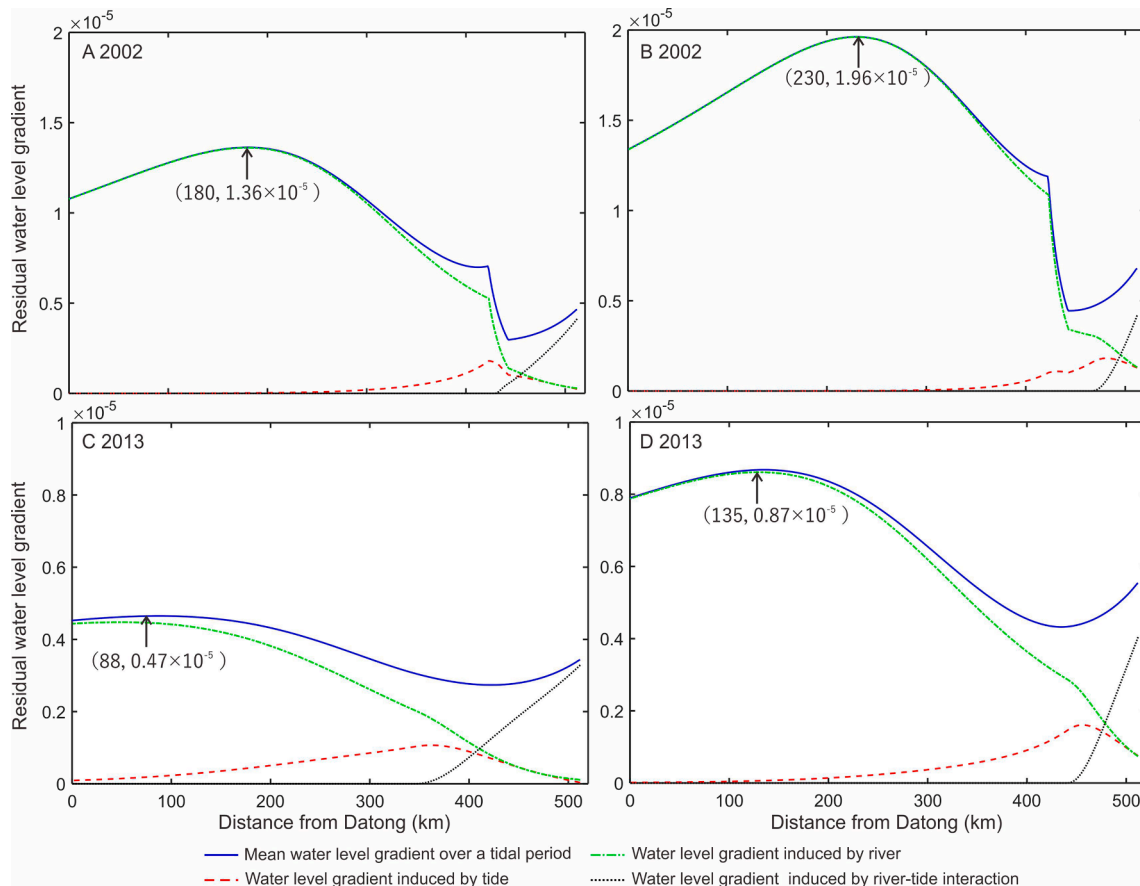
Fig. 8. Longitudinal variation of the residual water level slope, and the contributions of tidal and riverine forcing to the residual water level slope along the Datong-Xuliujing Reach for: (A, B) the period prior to the operation of the Three Gorges Dam and (C, D) the period after the operation of the Three Gorges Dam operation under (A, C) mean and (B, D) high fluvial discharge scenarios.

6.4. Limitations and way forward

The most restrictive assumption we have made in this study is to assume that the tidal wave can be described by a combination of a steady residual term (river discharge) and a time-dependent harmonic wave (tidal flow) in the analytical model. Thus the model can only deal with tide-river interactions for a single predominant tidal constituent and fails to capture any tidal asymmetry introduced by astronomical tides, overtides and compound tides. This is reasonable as the Changjiang estuary is dominated by the M_2 semi-diurnal tidal constituent, followed (in order of importance) by the S2, K1 and O1 constituents (Zhang et al., 2018). Located over 100 km away from the East China Sea, the DXR is affected by the tide mainly in terms of water level fluctuation, rather than tidal asymmetry, similar to the tidal reach of the alluvial Mississippi River (Wang and Xu, 2018). As Figs. 6 and 8 indicates, the residual water level gradient reaches its maximum value at a location between 88 and 246 km from Datong, depending on the magnitude of the varying fluvial discharge. Over this range the tidal amplitudes of S2, K1 and O1 are all very small and their fluctuations can be considered negligible (Zhang et al., 2018). In addition, the analytical model is based on a tidally-averaged scale rather than considering time varying processes caused by tidal action, it therefore fails to deduct the bed shear stress profile and cannot be used to detect sediment transport along the channel directly. The focus on such a time scale is acceptable in this study, given the long interval between the available bathymetric surveys and the limited effects of tidal asymmetry on the tidal reach. Furthermore, although the erosion and accretion patterns along the estuary are strongly related to the shape of the residual water level profile (Lamb et al., 2012; Cai et al., 2019), further studies and investigations are necessary to directly determine the mechanisms of net transport of sediment and thus directly link the tide-river dynamics to the tidal reach morphology.

7. Conclusions

The tidal reach is a vital component of a river system, which directly links the upstream river basin with the outer estuary. Influenced by both fluvial discharge and water level fluctuations due to tidal action, the erosion/accretion states of a tidal reach have their own unique properties that contrast sharply with those of the river and estuary. Using a case study of the DXR in the tidal reach of the Changjiang River, this study has revealed the response of channel morphology to both river-tide interactions and anthropogenic disturbances. The main conclusions are as follows:

1. The DXR experienced dramatic variations in morphology during 1992–2013, with a net accretion of 0.04 m/y during 1992–2002, a net erosion of 0.03 m/y during 2002–2008, and again a net accretion of 0.07 m/y during 2008–2013. The accretion status during 1992–2002 and 2008–2013 both exhibit a distinct Gaussian variation with respect to distance along the channel.

2. Despite a rapid decrease in fluvial sediment supply due to the construction of the Three Gorges Dam (TGD) in 2003, the DXR exhibits a clear maximum accretion zone during 1992–2002 and 2008–2013, respectively, when the river-tide dynamics dominate the channel morphology along DXR. In the natural scenario, during 1992–2002, the DXR exhibited a zone of maximum accretion that was located around 230–280 km downstream of Datong; but this zone subsequently shifted ~ 100 km landwards during 2008–2013.

3. The considerable decrease in high flow discharge during the wet season following the seasonal operation of TGD for flood control is primarily responsible for the observed landward shift of the maximum accretion zone within the DXR. However, the intrinsic characteristics of the local geomorphologic configuration generate spatial nonuniformity in the overall pattern of erosion/deposition, with localized sand mining and dredging projects in particular causing occasional outliers of significant erosion/deposition.

Declaration of Competing Interest

The authors declare that they have no known competing financial interests or personal relationships that could have appeared to influence the work reported in this paper.

Appendix A. Supplementary data

Supplementary data to this article can be found online at https://doi.org/10.1016/j.jhydrol.2020.125789.

References

Angamuthu, B., Darby, S.E., Nicholls, R.J., 2018. Impacts of natural and human drivers on the multi-decadal morphological evolution of tidally-influenced deltas. P. Roy. Soc. A-Math Phys. 474 (2219), 20180396.

Assani, A.A., Landry, R., Daigle, J., Chalifour, A., 2011. Reservoirs effects on the interannual variability of winter and spring streamflow in the St-Maurice River Watershed (Quebec, Canada). Water Resour. Manage. 25 (14), 3661–3675.

Auerbach, L., Goodbred Jr., S., Mondal, D., et al., 2015. Flood risk of natural and embanked landscapes on the Ganges-Brahmaputra tidal delta plain. Nat. Clim. Change 5 (2), 153–157.

Bain, R.L., Hale, R.P., Goodbred, S.L., 2019. Flow reorganization in an anthropogenically modified tidal channel network: an example from the southwestern Ganges-Brahmaputra-Meghna Delta. J. Geophys. Res.-Earth. 124, 2141–2159.

Bao, Y.H., Gao, P., He, X., 2015. The water-level fluctuation zone of Three Gorges Reservoir — A unique geomorphological unit. Earth-Sci. Rev. 150, 14–24.

Best, J., 2018. Anthropogenic stresses on the world's big rivers. Nat. Geosci. 12, 7–21.

Blott, S.J., Pye, K., van der Wal, D., Neal, A., 2006. Long-term morphological change and its causes in the Mersey Estuary, NW England. Geomorphology 81, 185–206.

Bunte, K., Abt, S.R., Swingle, K.W., Cenderelli, D.A., 2014. Effective discharge in Rocky Mountain headwater streams. J. Hydrol. 2136–2147.

Cai, H.Y., Savenije, H.H.G., Toffolon, M., 2013. Linking the river to the estuary: influence of river discharge on tidal damping. Hydrol. Earth Syst. Sci. 18, 287–304.

Cai, H.Y., Savenije, H.H.G., Jiang, C., Zhao, L., Yang, Q., 2016. Analytical approach for determining the mean water level profile in an estuary with substantial fresh water discharge. Hydrol. Earth Syst. Sci. 20, 1177–1195.

Cai, H.Y., Savenije, H.H.G., Garel, E., Zhang, X.Y., Guo, L.C., Zhang, M., Liu, F., Yang, Q. S., 2019. Seasonal behaviour of tidal damping and residual water level slope in the Yangtze River estuary: identifying the critical position and river discharge for maximum tidal damping. Hydrol. Earth Syst. Sci. 18, 287–304.

Cai, H.Y., Zhang, P., Garel, E., Matte, P., Hu, S., Liu, F., Yang, Q.S., 2020. A novel approach for the assessment of morphological evolution based on observed water levels in tide-dominated estuaries. Hydrol. Earth Syst. Sci. 24, 1871–1889.

Calle, M., Alho, P., Benito, G., 2017. Channel dynamics and geomorphic resilience in an ephemeral mediterranean river affected by gravel mining. Geomorphology 285, 333–346.

Chen, J., Finlayson, B.L., Wei, T., Sun, Q., Webber, M., Li, M., Chen, Z., 2016. Changes in monthly flows in the Yangtze River, China – With special reference to the Three Gorges Dam. J. Hydrol. 536, 293–301.

Chen, X.Q., Zhou, Q.J., Zhang, E.F., 2006. In-channel sand extraction from the midlower Yangtze channels and its management: problems and challenges. J. Environ. Plann. Man. 49 (2), 309–320.

Dai, Z.J., Liu, J.T., Wei, W., Chen, J.Y., 2014. Detection of the Three Gorges Dam influence on the Changjiang (Yangtze River) submerged delta. Sci. Rep. 4, 6600.

Dai, Z.J., Fagherazzi, S., Mei, X., Gao, J.J., 2016. Decline in suspended sediment concentration delivered by the Changjiang (Yangtze) River into the East China Sea between 1956 and 2013. Geomorphology 268, 123–132.

Dai, Z.J., Fagherazzi, S., Gao, S., Mei, X., Ge, Z.P., Wei, W., 2018. Scaling properties of estuarine beaches. Mar. Geol. 404, 130–136.

Deng, S.S., Xia, J.Q., Zhou, M.R., Lin, F.F., 2019. Coupled modeling of bed deformation and bank erosion in the Jingjiang Reach of the Middle Yangtze River. J. Hydrol. 568, 221–233.

Darby, S.E., Hackney, C.R., Leyland, J., et al., 2016. Fluvial sediment supply to a mega-delta reduced by shifting tropical-cyclone activity. Nature 539 (7628), 276–279.

Doyle, M.W., Stanley, E.H., Strayer, D.L., et al., 2005. Effective discharge analysis of ecological processes in streams. Water Resour. Res. 41, W11411.

Dronkers, J.J., 1964. Tidal Computations in River and Coastal Waters. Elsevier, New York, pp. 1–518.

Du, J.L., Yang, S.L., Feng, H., 2016. Recent human impacts on the morphological evolution of the Yangtze River delta foreland: a review and new perspectives. Estuar. Coast. Shelf Sci. 181, 160–169.

Dunn, F., Darby, S., Nicholls, R., Cohen, S., Zarfl, C., Fekete, B., 2019. Projections of declining fluvial sediment delivery to major deltas worldwide in response to climate change and anthropogenic stress. Environ. Res. Lett. 14 (8), 1–11.

Ericson, J.P., Vörösmarty, C.J., Dingman, S.L., Ward, L.G., Meybeck, M., 2006. Effective sea-level rise and deltas: causes of change and human dimension implications, Global Planet. Change 50, 63–82.

Giosan, L., Constantinescu, S., Filip, F., Deng, B., 2013. Maintenance of large deltas through channelization: nature vs. humans in the Danube delta. Anthropocene 1, 35–45.

Giosan, L., Syvitski, J., Constantinescu, S., Day, J., 2014. Climate change: protect the world's deltas. Nature 516, 31–33.

Hackney, C.R., Darby, S.E., Parsons, D.R., et al., 2020. River bank instability from unsustainable sand mining in the lower Mekong River. Nat. Sustain. 3, 217–225.

Hoitink, A.J.F., Wang, Z.B., Vermeulen, B., Huismans, Y., Kästner, K., 2017. Tidal controls on river delta morphology. Nat. Geosci. 10, 637–645.

Kondolf, G.M., Rubin, Z.K., Minear, J.T., 2014. Dams on the Mekong: cumulative sediment starvation. Water Resour. Res. 50, 5158–5169.

Kuang, C., Liu, X., Gu, J., et al., 2013. Numerical prediction of medium-term tidal flat evolution in the Yangtze estuary: impacts of the Three Gorges project. Cont. Shelf Res. 52, 12–26.

Lai, X., Yin, D., Finlayson, B.L., Wei, T., Li, M., Yuan, W., et al., 2017. Will river erosion below the Three Gorges Dam stop in the middle Yangtze? J. Hydrol. 554, 24–31.

Lamb, M.P., Nittrouer, J.A., Mohrig, D., Shaw, J., 2012. Backwater and river plume controls on scour upstream of river mouths: Implications for fluvio-deltaic morphodynamics. J. Geophys. Res.-Earth. 117, F01002.

Lauri, H., de Moel, H., Ward, P.J., Rasanen, T.A., Keskinen, M., Kummu, M., 2012. Future changes in Mekong River hydrology: impact of climate change and reservoir operation on discharge. Hydrol. Earth Syst. Sci. 16 (12), 4603–4619.

Lentsch, N., Finotello, A., Paola, C., 2018. Reduction of deltaic channel mobility by tidal action under rising relative sea level. Geology 46, 599–602.

Leonardi, N., Kolker, A.S., Fagherazzi, S., 2015. Interplay between river discharge and tides in a delta distributary. Adv. Water Resour. 80, 69–78.

Liu, G.P., Xu, H., Bi, J.F., 2014. Sand dredging along the Jiangsu Reach of Changjing River and their effects. Yangtze River s2, 193–196.

Luan, H.L., Ding, P.X., Wang, Z.B., Ge, J.Z., 2017. Process-based morphodynamic modeling of the Yangtze estuary at a decadal timescale: Controls on estuarine evolution and future trends. Geomorphology 290, 347–364.

Mei, X., Dai, Z., van Gelder, P.H.A.J.M., Gao, J., 2015. Linking three gorges dam and downstream hydrological regimes along the yangtze river, China. Earth Space Sci. 2 (4), 94–106.

Mei, X., Du, J., Dai, Z., Du, J., Gao, J., Wang, J., 2018. Decadal sedimentation in China's largest freshwater lake, Poyang Lake. Geochem. Geophy. Geosy. 19, 2384–2396.

Mei, X., Zhang, M., Dai, Z., Wei, W., Li, W.H., 2019. Large addition of freshwater to the tidal reaches of the Yangtze (Changjiang) River. Estuar. Coast. 42, 629–640.

Montreuil, A., Levoy, F., Bretel, P., Anthony, E.J., 2014. Morphological diversity and complex sediment recirculation on the ebb delta of a macrotidal inlet (Normandy, France): a multiple LiDAR dataset approach. Geomorphology 219, 114–125.

Nienhuis, J.H., Hoitink, A.J.F.T., Törnqvist, T.E., 2018. Future change to tide-influenced deltas. Geophys. Res. Lett. 45 (8), 3499–3507.

Nicholls, R.J., Hutton, C.W., Lázár, A.N., et al., 2016. Integrated assessment of social and environmental sustainability dynamics in the Ganges-Brahmaputra-Meghna Delta, Bangladesh. Estuar. Coast. Shelf Sci. 183, 370–381.

Paola, C., Twilley, R.R., Edmonds, D.A., et al., 2011. Natural processes in delta restoration: application to the mississippi delta. Annu. Rev. Mar. Sci. 3, 67–91.

Poff, N.L., Olden, J.D., Merritt, D.M., Pepin, D.M., 2007. Homogenization of regional river dynamics by dams and global biodiversity implications. Proc. Natl. Acad. Sci. U.S.A. 104 (14), 5732–5737.

Rahman, M., Dustegir, M., Karim, R., et al., 2018. Recent sediment flux to the ganges-brahmaputra-meghna delta system. Sci. Total Environ. 643, 1054–1064.

Räsänen, T.A., Someth, P., Lauri, H., et al., 2017. Observed river discharge changes due to hydropower operations in the upper mekong basin. J. Hydrol. 545, 28–41.

Rouse, H., 1961. Fluid Mechanics for Hydraulic Engineers. Dover Publications Inc, New York.

Sassi, M.G., Hoitink, A.J.F., 2013. River flow controls on tides and tide-mean water level profiles in a tidal freshwater river. J. Geophys. Res. -Oceans 118 (9), 4139–4151.

Savenije, H.H.G., 2012. Salinity and Tides in Alluvial Estuaries, 2nd ed. Elsevier, New York.

Syvitski, J.P.M., Kettner, A.J., Overeem, I., et al., 2009. Sinking deltas due to human activities. Nat. Geosci. 2, 681–686.

Tessler, Z.D., Vörösmarty, C.J., Grossberg, M., et al., 2015. Profiling risk and sustainability in coastal deltas of the world. Science 349, 638–643.

The Ministry of Water Resources of the People's Republic of China (MWRPRC), 2012. Code for hydrologic data processing. China Water Power Press, Beijing.

Toffolon, M., Vignoli, G., Tubino, M., 2006. Relevant parameters and finite amplitude effects in estuarine hydrodynamics. J. Geophys. Res. -Oceans 111, C10014.

Van der Wal, D., Pye, K., Neal, A., 2002. Long-term morphological change in the Ribble Estuary, northwest England. Mar. Geol. 189, 249–266.

Wang, B., Xu, Y. J., 2018. Decadal-scale riverbed deformation and sand budget of the last 500 km of the Mississippi River: Insights into natural and river engineering effects on a large alluvial river, J. Geophys. Res.-Earth., 123.

Wolman, M.G., Miller, J.P., 1960. Magnitude and frequency of forces in geomorphic processes. J. Geol. 68, 54–74.

Yan, W., Mayorga, E., Li, X., Seitzinger, S.P., Bouwman, A.F., 2010. Increasing anthropogenic nitrogen inputs and riverine DIN exports from the Changjiang River basin under changing human pressures. Global Biogeochem. Cycle 24 (4), GB0A06.

Yang, Y.P., Zhang, M.J., Liu, W.L., Wang, J.J., Li, X.X., 2019. Relationship between waterway depth and low-flow water levels in reaches below the Three Gorges Dam. J. Waterw. Port C-ASCE 145 (1), 04018032.

Yuan, W., Yin, D., Finlayson, B., Chen, Z., 2012. Assessing the potential for change in the middle Yangtze River channel following impoundment of the Three Gorges Dam. Geomorphology 147–148, 27–34.

Zhang, F.Y., Sun, J., Lin, B.L., Huang, G.X., 2018. Seasonal hydrodynamic interactions between tidal waves and river flows in the Yangtze Estuary, J. Marine Syst., 186, 17-28.Zhang, G., Cheng, W.C., Chen, L.H., Zhang, H., Gong, W.P., 2019. Transport of riverine sediment from different outlets in the Pearl River Estuary during the wet season, Mar. Geol., 415, 105957.

Zhang, M., Townend, I., Zhou, Y., Cai, H., 2016. Seasonal variation of river and tide energy in the Yangtze estuary, China. Earth Surf. Proc. Land. 41 (1), 98–116.

Zhang, X., Fagherazzi, S., Leonardi, N., Li, J.F., 2018. A positive feedback between sediment deposition and tidal prism may affect the morphodynamic evolution of tidal deltas. J. Geophys. Res.-Earth. 123, 2767–2783.

Zheng, S.W., Xu, Y.J., Cheng, H.Q., Wang, B., Xu, W., Wu, S.H., 2018. Riverbed erosion of the final 565 kilometers of the Yangtze River (Changjiang) following construction of the Three Gorges Dam. Sci. Rep. 8, 11917.

Zhou, Z., Coco, G., Townend, I., Gong, Z., Wang, Z.B., Zhang, C.K., 2018. On the stability relationships between tidal asymmetry and morphologies of tidal basins and estuaries. Earth Surf. Proc. Land. 43, 1943–1959.